Journal of Materials Science & Technology 34 (2018) 1781–1790

Contents lists available at ScienceDirect

Journal of Materials Science & Technology

journal homepage: www.jmst.org

Effect of nitrogen on corrosion behaviour of a novel high nitrogen medium-entropy alloy CrCoNiN manufactured by pressurized metallurgy

Hao Feng[a], Huabing Li[a,*], Xiaolei Wu[b,*], Zhouhua Jiang[a], Si Zhao[a], Tao Zhang[c], Dake Xu[c], Shucai Zhang[a], Hongchun Zhu[a], Binbin Zhang[a], Muxin Yang[b]

[a] School of Metallurgy, Northeastern University, Shenyang 110819, China
[b] State Key Laboratory of Nonlinear Mechanics, Institute of Mechanics, Chinese Academy of Sciences, Beijing 100190, China
[c] School of Materials Science and Engineering, Northeastern University, Shenyang 110819, China

ARTICLE INFO

Article history:
Received 28 December 2017
Received in revised form 31 January 2018
Accepted 6 March 2018
Available online 3 April 2018

Keywords:
Medium-entropy alloy
Nitrogen
Pitting corrosion
Passive film
Metastable pitting

ABSTRACT

A novel high nitrogen medium-entropy alloy CrCoNiN, which had higher strength and slightly lower ductility than CrCoNi alloy, was successfully manufactured by pressurized metallurgy. The microstructure and corrosion behaviour were investigated by microscopic, electrochemical and spectroscopic methods. The results indicated that nitrogen existed in the form of Cr_2N precipitates and uniformly distributed N atoms, and nitrogen alloying significantly refined the grain size. Besides, nitrogen enriched on the outmost surface of passive film and metal/film interface as ammonia (NH_3 and NH_4^+) and CrN, respectively. The significant improvement of corrosion resistance of CrCoNiN was attributed to the lower metastable pitting susceptibility together with thicker, less defective and more compact passive film.

1. Introduction

The newly explored high-entropy alloys, being composed of multiple principle elements in equimolar or near-equimolar ratio [1], have drawn extensive attentions [2,3]. In recent years, various high-entropy alloys have been developed which exhibit excellent combination of strength and ductility especially at low temperature [4,5], high wear resistance [6] and good thermal stability [7], etc. The three-component CrCoNi medium-entropy alloy, which has low mixing configurational entropy ($\triangle S_{conf} = 1.10R$), possesses high work hardenability, excellent ductility and fracture resistance [5,8]. However, considering the demand for engineering application, it may not satisfy the requirement of high yield strength at elevated temperatures [9,10]. Therefore, mechanical alloying together with spark plasma sintering (MA + SPS) [9] and precipitation hardening by adding a small amount of Al and Ti [10] were investigated to increase the strength of CrCoNi alloy. Besides, as an important strengthening mechanism, interstitial strengthening by boron [11] and carbon [12] has be adopted to improve the mechanical properties of high-entropy alloys. However, both elements deteriorated the properties of alloys because boron worsened the corrosion resistance [13] and carbon promoted the sensitivity of precipitation [14].

The beneficial effects of nitrogen on mechanical properties of austenitic [15–18], duplex [19,20] and martensitic [21,22] stainless steels have been widely reported. Besides, nitrogen in stainless steels could decrease the metastable pitting susceptibility [16], promote passivation and stability of passive film [15,23,24], thus enhancing the corrosion resistance of stainless steels [25]. Therefore, it can be inferred that nitrogen has a great potential in improving the properties of CrCoNi medium-entropy alloy. Considering the extremely low nitrogen solubility in Ni and Co based alloys at atmospheric pressure [26], pressurized metallurgy, as an effective technique to enhance nitrogen content in stainless steels and alloys [21,27,28], has been firstly used to manufacture the novel high nitrogen medium-entropy alloy CrCoNiN by the authors. Recently, Wu [29] reported that the CrCoNiN alloy exhibited an obvious increase in strength and a slight decrease in ductility compared with CrCoNi alloy (Table 1). However, the effect of nitrogen on corrosion resistance of CrCoNiN alloy is still unclear.

* Corresponding authors.
E-mail addresses: huabing_li@163.com (H. Li), xlwu@imech.ac.cn (X. Wu).

https://doi.org/10.1016/j.jmst.2018.03.021
1005-0302/

Table 1
Chemical compositions and mechanical properties of the investigated medium-entropy alloys.

	Chemical composition					Mechanical properties (at 25 °C)		
Alloys		Cr	Co	Ni	N	Yield strength (MPa)	Ultimate tensile strength (MPa)	Elongation (%)
CrCoNi	wt%	30.58	34.71	34.71	–	205.6	638.6	68.9
	at%	33.25	33.31	33.44	–			
CrCoNiN	wt%	30.45	34.56	34.55	0.44	374.4	1161.1	43.0
	at%	32.68	32.73	32.84	1.75			

The aim of the present paper is to reveal the effect of nitrogen on microstructure and corrosion resistance of CrCoNiN alloy. The microstructure characterizations were analysed employing optical microscope (OM), field emission scanning electron microscope (FE-SEM), transmission electron microscope (TEM) and three-dimensional atom probe (3DAP). The corrosion resistance was investigated by potentiodynamic and cyclic polarization together with critical pitting temperature (CPT) tests. In addition, characteristic of passive film was analysed with Mott-Schottky and X-ray photoelectron spectrometer (XPS) analyses. Finally, the effects of nitrogen on passive film and metastable pitting initiation on CrCoNi alloy were discussed.

2. Experimental procedure

2.1. Materials and heat treatment

The CrCoNi and CrCoNiN medium-entropy alloys were produced from high purity elements Cr (99.17%), Co (99.98%) and Ni (99.96%) in a 25 kg pressurized induction furnace. The CrCoNi alloy was melted and poured into ingot mould under argon atmosphere, and the CrCoNiN alloy was melted and poured under nitrogen pressure of 1.0 MPa and 2.0 MPa, respectively. Before pouring, nickel magnesium (NiMg) master alloy and metallic cerium (Ce) were added into the melt for deoxidization and desulfurization. Nitrogen was added into CrCoNiN alloy through gas nitriding during melting and pouring under high nitrogen pressure. The chemical compositions of the alloys are shown in Table 1. Then the heat treatment and hot working processes were performed using a muffle furnace under air atmosphere. The ingots were homogenized at 1200 °C for 24 h, and then hot forged to 70 mm × 12 mm plates in the temperature range of 1200 °C–950 °C. Finally, the plates were solution treated at 1150 °C for 2 h followed by water quenching.

2.2. Microstructure observation

The specimens with dimensions of 10 mm × 10 mm × 6 mm were machined from the plates. They were wet ground with successive grade SiC papers up to 2000 grit, polished with 1.5 μm diamond paste, and then etched using the reagent consisting of 1 g $FeCl_3$ + 5 mL HCl + 1 mL HNO_3 + 10 mL H_2O. The microstructure of the specimens were observed using an Olympus DSX510 optical microscope (OM) and a Carl-Zeiss Ultra Plus field emission scanning electron microscope (FE-SEM) equipped with an energy dispersive spectroscopy (EDS) system. Thin foils for transmission electron microscopy (TEM) observation were mechanically ground with SiC paper to the thickness of 30 μm and punched into discs with the diameter of 3 mm. After that, the discs were Ar-ion milled and then analysed using an FEI Tecnai F30 microscope. To investigate the elemental distribution in CrCoNiN alloy, the three-dimensional atom probe (3DAP) analysis was performed with a Cameca local electrode atom probe (LEAP 4000X HR). The data were reconstructed and analysed with Imago Visualization and Analysis Software (IVAS™ 3.6.8).

2.3. Electrochemical measurements

The electrochemical measurements were conducted using a Gamry Reference 600 potentiostat with a three-electrode cell. The working electrode was mounted in epoxy resin with an exposure area of 1.0 cm^2, and then abraded with SiC papers up to 2000 grit before the experiments. A platinum plate was served as the counter electrode and a saturated calomel electrode (SCE) as the reference electrode. The electrolyte was 3.5 wt% NaCl solution in naturally aerated condition, and the temperature was maintained at 30 °C, 50 °C and 70 °C in water bath. Prior to the electrochemical measurements, the working electrode was cathodically polarized at −1.0 V_{SCE} for 5 min to remove the air formed oxide layer and then stabilized in the electrolyte for 30 min to achieve the steady state condition. The potentiodynamic polarization test was performed at a sweep rate of 0.333 mV/s from −0.3 V below open circuit potential (OCP) in the anodic direction, and the test was terminated when the current density exceeded 1 mA/cm^2. The cyclic polarization test was carried out at a sweep rate of 1 mV/s from −0.3 V below OCP, and the scan was reversed to the starting potential when the current density reached 1 mA/cm^2. The pitting potential (E_{pit}) was determined when the current density reached 100 μA/cm^2. The potentiostatic measurement was carried out to measure the critical pitting temperature (CPT). The anodic potential of 600 mV_{SCE} was applied to the working electrode, and the electrolyte temperature was increased at the rate of 1 °C/min with the initial temperature of 10 °C. The CPT was defined as the temperature at which the current density reached 100 μA/cm^2 and stayed above this value for 60 s [30].

In order to examine the semiconductor property of the passive film, Mott-Schottky measurement was preformed after forming the passive film at 0 mV_{SCE} for 3600 s. The Mott-Schottky measurement was carried out at a fixed frequency of 1000 Hz using a 5 mV amplitude voltage. The potential sweep was performed at a step rate of 25 mV in the passive zone according to the potentiodynamic polarization curves. All the electrochemical measurements were repeated three times.

2.4. XPS analysis

The working electrodes for passive film analyses were polished with 1.5 μm diamond paste. The passive films on CrCoNi and CrCoNiN alloys were formed under the potential of 0 mV_{SCE} for 3600 s at 50 °C after the air formed oxide layer was removed. X-ray photoelectron spectrometer (XPS) was employed to analyse the chemical composition of the passive film using ESCALAB250 equipped with Al Kα (1486.6 eV, 150 W) X-ray source, and the photoelectron take-off angle was 90°. The depth profile information was obtained using argon ions sputtering (base pressure: 1.33×10^{-5} Pa, energy: 2 keV, current: 2.0 μA/cm^2) over an area of 2 mm × 2 mm. XPS survey spectra were recorded to identify the elements in the passive film, and then the high resolution spectra of Cr 2p, Ni 2p, Co 2p, O 1s, N 1s and C 1s were recorded. The binding energies were corrected according to the internal standard of C 1s peak at 284.6 eV. The spectra were fitted using XPSPEAK 4.0 software by reference to a database [31].

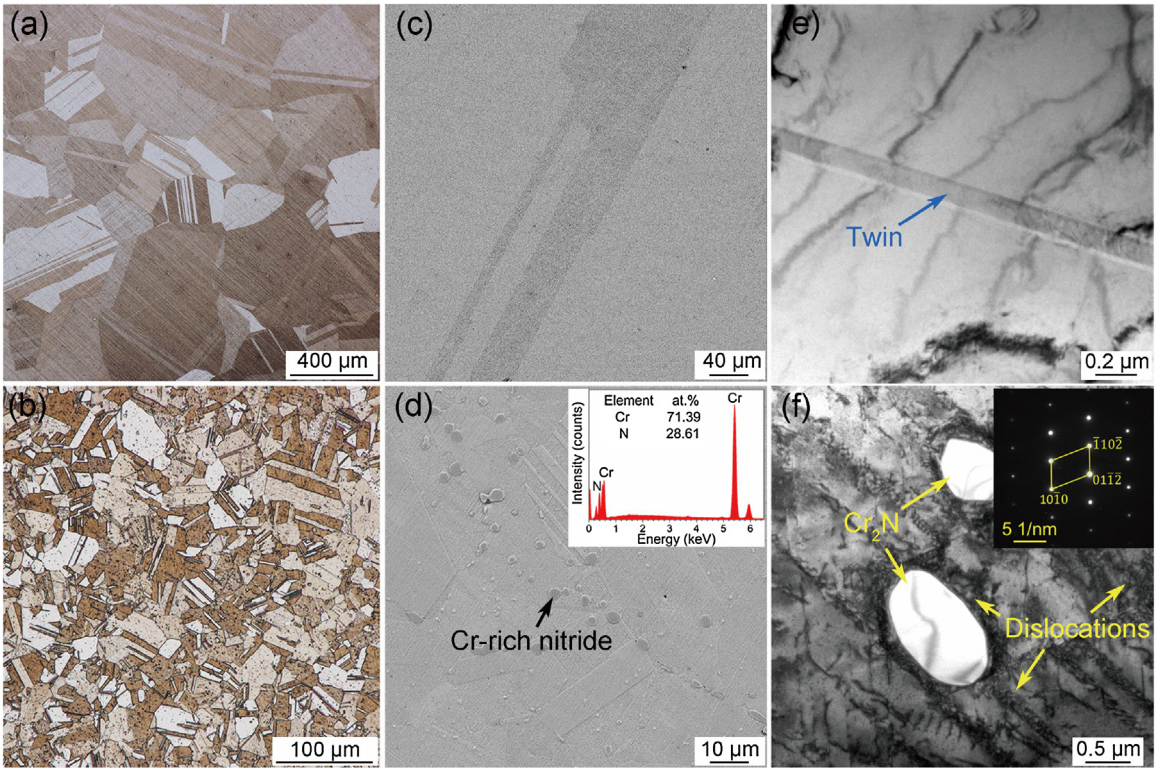

Fig. 1. OM, SEM and TEM micrographs of (a), (c), (e) CrCoNi and (b), (d), (f) CrCoNiN medium-entropy alloys.

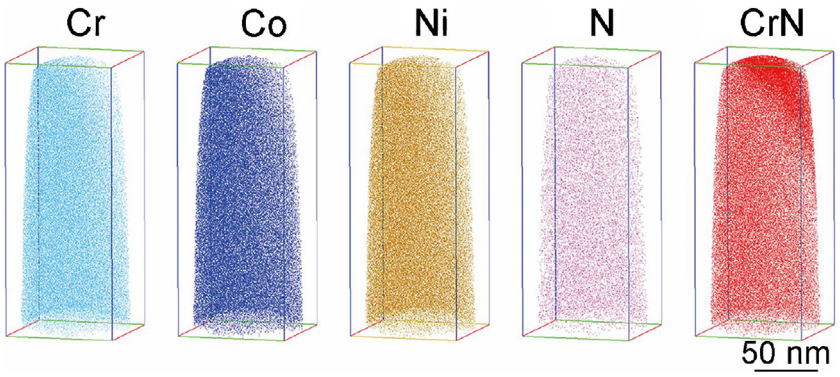

Fig. 2. 3D atom-by-atom tomographic reconstruction (box size 87 nm × 87 nm × 216 nm) of CrCoNiN medium-entropy alloy.

3. Results

3.1. Microstructure characterizations

The OM micrographs of CrCoNi and CrCoNiN medium-entropy alloys are shown in Fig. 1(a) and (b). The microstructure of both alloys consisted of austenite grains with annealing twins, and the grains were remarkably refined by nitrogen alloying. The SEM micrographs (Fig. 1(c) and (d)) show that no precipitate existed in CrCoNi alloy, whereas massive precipitates were observed in CrCoNiN alloy. Based on the chemical composition of precipitates by EDS analysis, the precipitates were preliminarily determined to be Cr-rich nitrides. The TEM micrograph of CrCoNi alloy in Fig. 1(e) reveals annealing twin with very low dislocation density. However, the CrCoNiN alloy (Fig. 1(f)) exhibits a high dislocation density especially around the precipitates. Besides, the precipitates in CrCoNiN alloy were confirmed to be Cr_2N according to the SAD pattern. Based on the microstructure observation, the addition of nitrogen obviously reduced the austenite grain size and induced the formation of Cr_2N precipitates together with high dislocation density.

The 3D atom-by-atom tomographic reconstruction of CrCoNiN medium-entropy alloy is illustrated in Fig. 2. It indicates that the Cr, Co, Ni and N elements were almost uniformly distributed in the alloy. It is noteworthy that both uniform distribution and segregation of CrN were observed. The existence of uniformly distributed CrN was attributed to the field evaporation of N atom together with Cr atom, and the segregated CrN was ascribed to Cr_2N precipitate. Therefore, nitrogen exists in CrCoNiN alloy in the form of Cr_2N precipitates and uniformly distributed N atoms.

3.2. Electrochemical measurements

Fig. 3(a) and (b) shows the potentiodynamic polarization curves of CrCoNi and CrCoNiN medium-entropy alloys, respectively. The CrCoNi alloy exhibited a wide passive range at 30 °C in which the current density kept almost stable. As the temperature increased

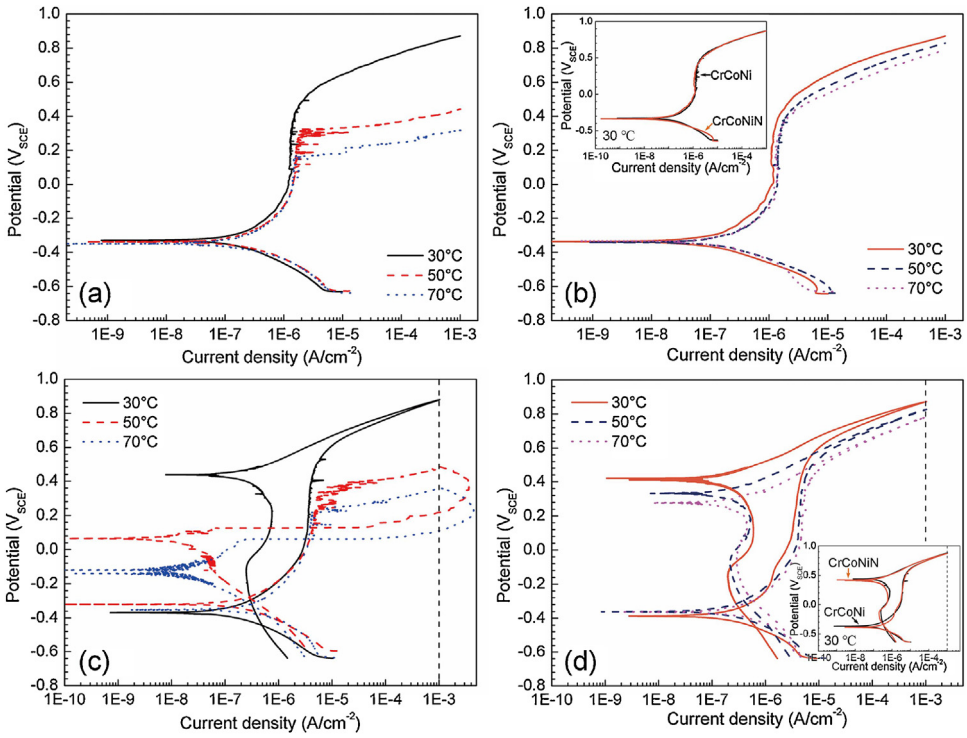

Fig. 3. Potentiodynamic polarization curves and cyclic polarization curves of (a)(c) CrCoNi and (b)(d) CrCoNiN medium-entropy alloys.

Table 2
Potentiodynamic and cyclic polarization parameters of the investigated medium-entropy alloys.

Alloys	Temperature (°C)	Potentiodynamic polarization		Cyclic polarization		
		$I_{corr} \times 10^7$ (A/cm^2)	E_{pit} (mV$_{SCE}$)	E_{pit} (mV$_{SCE}$)	E_{rp} (mV$_{SCE}$)	I_{max} (mA/cm^2)
CrCoNi	30	1.40 ± 0.33	744.9 ± 2.6	762.8 ± 2.2	E_{pit}	1.1 ± 0.0
	50	2.85 ± 0.34	336.7 ± 24.6	421.3 ± 8.1	147.3 ± 19.2	3.4 ± 0.2
	70	3.18 ± 0.96	240.7 ± 16.1	270.0 ± 10.5	55.3 ± 6.8	3.6 ± 0.9
CrCoNiN	30	1.39 ± 0.35	782.4 ± 9.7	763.1 ± 1.3	E_{pit}	1.0 ± 0.0
	50	2.34 ± 0.44	712.0 ± 8.7	711.6 ± 4.0	E_{pit}	1.0 ± 0.0
	70	2.75 ± 0.77	663.4 ± 35.1	660.9 ± 0.8	E_{pit}	1.0 ± 0.0

to 50 °C and 70 °C, the passive regions became narrow, and corrosion current densities (I_{corr}) increased and the pitting potentials (E_{pit}) decreased substantially (Table 2), which meant that the passive films degraded and the corrosion resistance decreased with the increasing of temperature. Moreover, current transients caused by activation and repassivation of metastable pitting [32] were observed, particularly at higher temperatures. The CrCoNiN alloy displays similar polarization behaviour with CrCoNi alloy at 30 °C, as shown in the inserted micrograph in Fig. 3(b). However, with the increasing of temperature, the corrosion current densities increased and pitting potentials decreased slightly (Table 2), and thus the passive film kept almost stable at high temperatures. Besides, the addition of nitrogen in CrCoNi alloy reduced the incidence of current transients. Therefore, it can be concluded that nitrogen alloying could inhibit the metastable pitting and enhance the pitting corrosion resistance of CrCoNiN alloy in high temperature chloride solution.

Fig. 3(c) and (d) shows the cyclic polarization curves of CrCoNi and CrCoNiN medium-entropy alloys. For CrCoNi alloy at 30 °C, the current density of the backward scan was lower than upward scan and the hysteresis loop did not appeared, which did not exhibit any pitting susceptibility. With increasing the temperatures to 50 °C and 70 °C, the current densities continuously increased to maximum current densities (I_{max}) in the backward scans and hysteresis loops were generated. The I_{max} increased and repassivation potential (E_{rp}) decreased with increasing temperature (Table 2), indicating the repassivation ability decreased and the pitting susceptibility increased at higher temperatures [33]. However, for CrCoNiN alloy, the cyclic polarization curve almost coincided with CrCoNiN at 30 °C, which was in accordance with the potentiodynamic polarization curves. The absence of hysteresis loops at 50 °C and 70 °C meant that CrCoNiN alloy exhibited low pitting susceptibility even at high temperatures. Thus, the addition of nitrogen effectively improved the repassivation ability and reduced the pitting susceptibility.

To elucidate the resistance to stable pitting growth of CrCoNi and CrCoNiN medium-entropy alloys in chloride solution at high temperature, CPT measurements were performed by potentiostatic polarization at 600 mV$_{SCE}$ in 3.5 wt% NaCl solution, as shown in Fig. 4. The current densities of both alloys gradually increased with the rise in temperature. The further raising of temperature induced sharp increasing of current densities, which indicated the occurrence of stable pitting. The CPT values were determined to be 49.8 ± 3.7 °C and 79.0 ± 1.4 °C for CrCoNi and CrCoNiN alloys, respectively. Compared with some commercial stainless steels (Table 3) [30,34–37], the CrCoNi alloy exhibits good corrosion resistance, and the addition of nitrogen further enhances its corrosion resistance in high temperature chloride solution.

Table 3
Main alloying element contents and CPT values of commercial stainless steels in literatures.

Alloys	Contents of main alloying elements (wt%)				CPT (°C)	Testing solutions
	Cr	Mo	N	Ni		
304 [34]	18	/	/	9	4.6	1 M NaCl
316L [30]	17.13	2.15	/	12.7	17.2	3.5 wt% NaCl
904L [35]	20.06	4.32	/	25.04	51.1	1 M NaCl
2101DSS [36]	21.4	0.31	0.23	1.2	33	1 M NaCl
2304DSS [37]	23.23	0.42	0.12	4.8	33	1 M NaCl

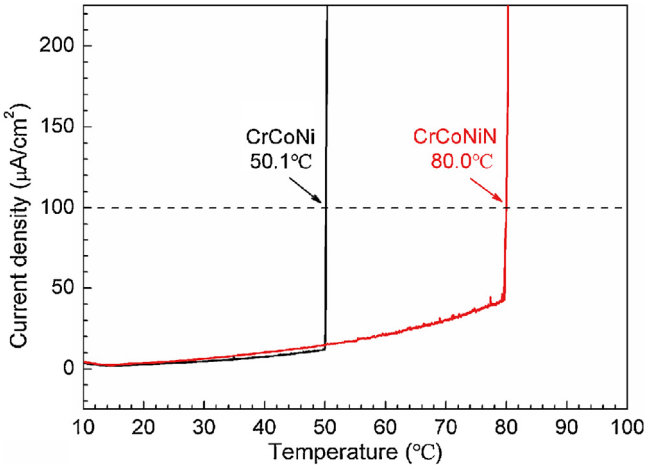

Fig. 4. Typical potentiostatic curves of CrCoNi and CrCoNiN medium-entropy alloys at 600 mV_{SCE} in 3.5 wt% NaCl solution.

3.3. Passive film analysis

Fig. 5(a) shows the Mott-Schottky plots for passive films on CrCoNi and CrCoNiN medium-entropy alloys formed at 0 mV_{SCE} for 3600 s in 3.5 wt% NaCl solution at different temperatures. The plots reveal that a linear relationship with a negative slope existed between $1/C^2$ and E, which agrees well with the Mott-Schottky equation for p-type semiconductor, as expressed by Eq. (1) [38–41]:

$$\frac{1}{C^2} = -\frac{2}{\varepsilon\varepsilon_0 q N_A}\left(E - E_{FB} - \frac{kT}{q}\right) \quad (1)$$

where C represents the space charge capacitance, ε the dielectric constant of the passive film (12.0), ε_0 the permittivity of free space (8.854×10^{-14} F/cm), q the electron charge (1.602×10^{-19}C), N_A the acceptor density, E_{FB} the flat band potential, k the Boltzmann constant (1.38×10^{-23} J/K), and T the absolute temperature. The N_A values of passive films on CrCoNi and CrCoNiN alloys determined from the slope of $1/C^2$ vs. E are all of the order of 10^{21} cm^{-3} (Fig. 5(b)), which are in similar range of stainless steels [39,42,43]. The N_A values for CrCoNi increased significantly with temperature, whereas the values for CrCoNiN slightly increased with temperature, and they were lower than CrCoNi alloy, especially at high temperatures. It indicates that the addition of nitrogen in CrCoNi alloy decreased the defect density, promoted the formation of less defective passive film and reduced its susceptibility to temperature.

Fig. 6(a) shows the XPS survey spectra of passive films on CrCoNi and CrCoNiN medium-entropy alloys. The elements Ni, Co, Cr, O and C were recorded on both alloys, but N was not observed on CrCoNiN alloy due to its low content. The ratios of Cr/(Cr + Ni + Co) in the passive films increased with the addition of nitrogen in CrCoNi alloy (Fig. 6(b)), and the enrichment of Cr could improve the stability and corrosion resistance of passive film [42]. The variation of O 1s contents in the passive films with etching time is displayed in Fig. 6(c), and the etching time when the O 1s content reached half of the maximum value was used to estimate the thickness of passive film [44,45]. Considering that the sputtering rate was about 0.2 nm/s (vs. Ta_2O_5) [46], the thickness of the passive films was increased from 3.56 nm for CrCoNi alloy to 5.61 nm for CrCoNiN alloy.

The XPS spectra of Cr $2p_{3/2}$, Co $2p_{3/2}$, Ni $2p_{3/2}$ and O 1s recorded from the outmost surface of passive films on CrCoNi and CrCoNiN medium-entropy alloys are illustrated in Fig. 7. The Cr $2p_{3/2}$ spectra were separated into $Cr(OH)_3$ (577.4 eV), Cr_2O_3 (576.0 eV) and Cr-met (574.0 eV). The Co $2p_{3/2}$ spectra were split into CoO (780.0 eV) and Co-met (778.1 eV). The Ni $2p_{3/2}$ spectra were dominated by $Ni(OH)_2$ (855.6 eV), NiO (854.0 eV) and Ni-met (852.6 eV), and the contents of $Ni(OH)_2$ and NiO were decreased by adding nitrogen into CrCoNi alloy. The O 1 s spectra were divided into OH^- (531.5 eV) and O^{2-} (529.8 eV), and hydroxides were the primary constituent on the outmost surface of the passive films.

Fig. 8 shows the XPS spectra of N 1 s recorded from the sputtering surfaces for 0 s, 10 s, 70 s and 170 s of the passive film on CrCoNiN alloy. On the outmost surface of the passive film, peaks representing NH_4^+ (400.3 eV), NH_3 (399.5 eV), Cr_2N (397.6 eV) and CrN (396.6 eV) were detected. After sputtering for 10 s, the peaks for NH_4^+ and NH_3 disappeared, and peaks representing Cr_2N and CrN increased. As the sputtering time prolonged to 70 s and 170 s, the intensity of CrN decreased, indicating that the nitrogen was enriched in the passive film in the form of CrN. However, the change

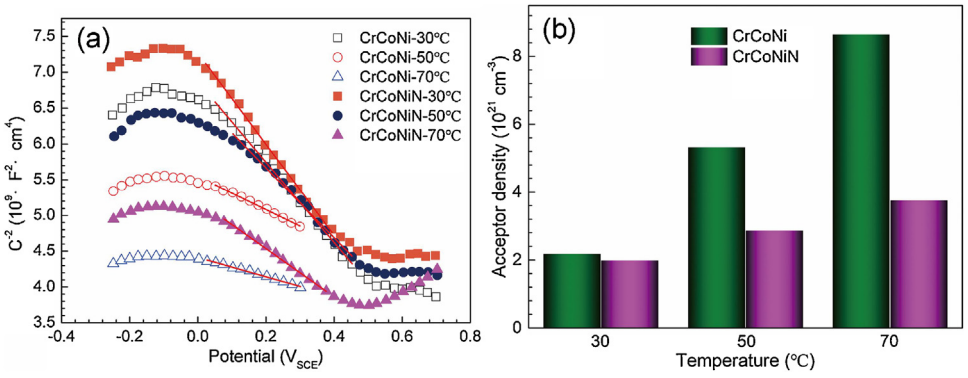

Fig. 5. (a) Mott-Schottky plots and (b) acceptor densities for passive films on CrCoNi and CrCoNiN medium-entropy alloys.

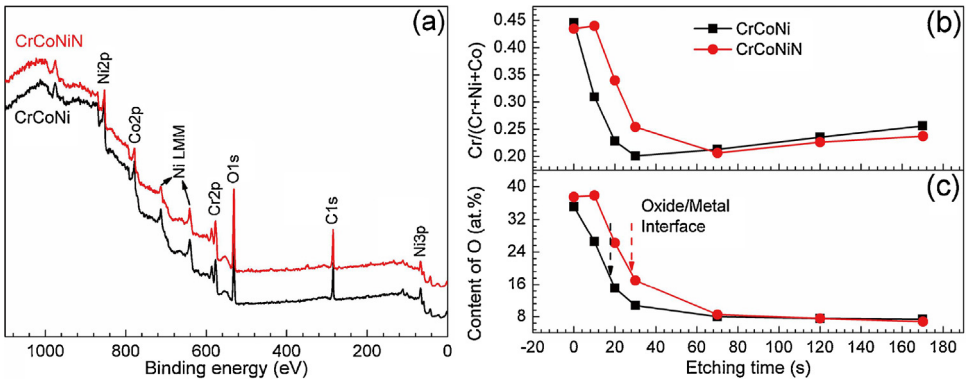

Fig. 6. (a) XPS spectra, (b) ratios of Cr/(Cr+Ni+Co) and (c) contents of O 1 s in the passive films on CrCoNi and CrCoNiN medium-entropy alloys.

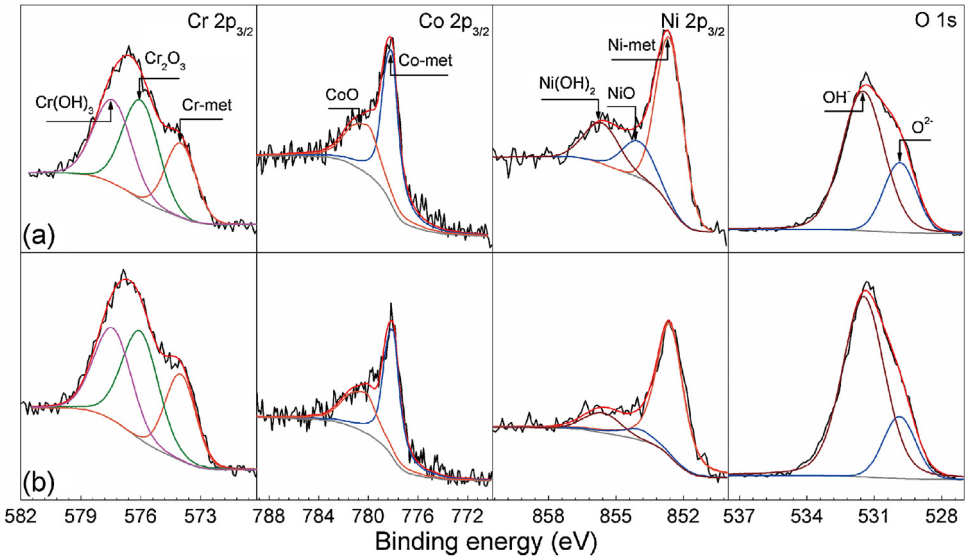

Fig. 7. XPS spectra of Cr $2p_{3/2}$, Co $2p_{3/2}$, Ni $2p_{3/2}$ and O 1 s recorded from the outmost surface of passive films on (a) CrCoNi and (b) CrCoNiN medium-entropy alloys.

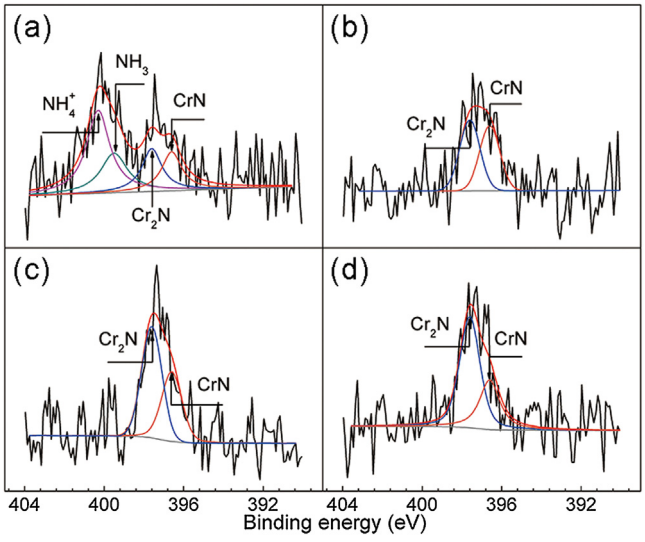

Fig. 8. XPS spectra of N 1 s recorded from the sputtering surfaces for (a) 0 s, (b) 10 s, (c) 70 s and (d) 170 s of the passive film on CrCoNiN medium-entropy alloy.

in intensity of Cr_2N with sputtering time was not obvious, which means that the Cr_2N in the passive film corresponded to Cr_2N precipitates which hardly changed with sputtering due to their large size.

4. Discussion

The addition of nitrogen in CrCoNi medium-entropy alloy induced the formation of Cr_2N precipitates and uniformly distributed N atoms, and then refined the grain size, reduced the defect density, enhanced the stability of passive film and significantly increased its corrosion resistance in high temperature chloride solution. Based on the above results, the effect of nitrogen on constitution, breakdown of passive film and the initiation of metastable pitting will be discussed in detail.

4.1. Effect of nitrogen on constitution of passive film

The significant increase in corrosion resistance of CrCoNiN medium-entropy alloy by adding nitrogen is closely related to the change in the constitution of passive film. The beneficial effects of nitrogen on passive films of austenitic and duplex stainless steels have been widely reported [15,43,47]. In the present study, the addition of nitrogen in CrCoNi alloy increased the thickness of passive film (Fig. 6(c)). However, Fu et al. [15] and Olefjord et al. [48] reported that nitrogen did not influence the thickness of passive film on austenitic stainless steels, which is inconsistent with our result. According to the work by Lee et al. [49] on 18Cr-10Mn-0.3C-0.3N austenitic stainless steel, the addition of Nb decreased the grain size and increased the thickness of passive film, which was regarded as one of the primary reasons for the enhanced

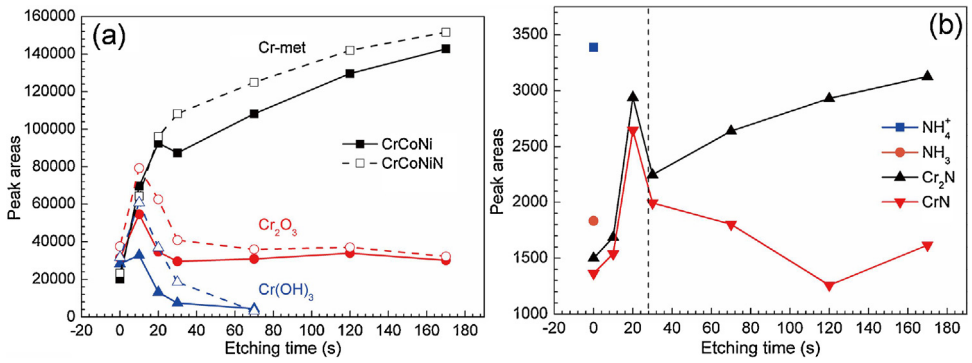

Fig. 9. Peak areas of species in (a) Cr $2p_{3/2}$ in the passive films on CrCoNi and CrCoNiN medium-entropy alloys and (b) N 1 s in the passive films on CrCoNiN alloy.

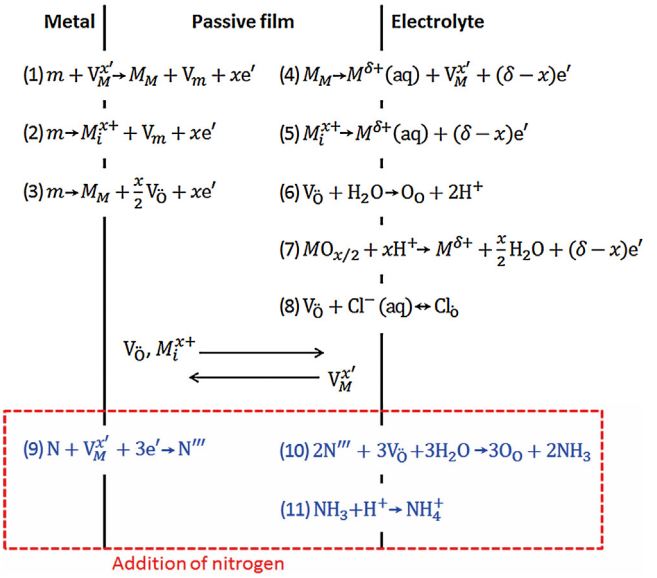

Fig. 10. Schematic diagram of physicochemical processes based on PDM model. m = metal atom, $V_M^{x'}$ = cation vacancy, M_M = metal cation in cation site, V_m = vacancy in metal site, M_i^{x+} = cation interstitial, $V_{\ddot{O}}$ = oxygen vacancy, $M^{\delta+}$ (aq) = metal cation in electrolyte, O_O = oxygen ion in anion site, Cl^- (aq) = chloride ion in electrolyte, $Cl_{\ddot{O}}$ = oxygen vacancy occupied by Cl^-, N = nitrogen atom, N‴ = nitrogen ion.

corrosion resistance. Therefore, considering that adding nitrogen significantly refined the grain size of CrCoNi alloy, the volume fraction of grain boundaries was increased, which further enhanced the passivation reaction due to the promoted diffusion of passive elements and the increased reactivity [49,50].

The enrichment of Cr in the passive films was observed on both CrCoNi and CrCoNiN alloys (Fig. 6(b)), and the addition of nitrogen further promoted the Cr enrichment, although the precipitation of Cr_2N in CrCoNiN alloy lowered the Cr content of the matrix. The promoted Cr enrichment and enhanced corrosion resistance by N was also reported by previous researchers on stainless steels [16,20,43,51]. As shown in Table 4, Ni and Co elements in the passive films on both alloys were depleted due to the higher diffusion rates of Co^{2+} and Ni^{2+} than that of Cr^{3+} [52], indicating that the preferential dissolution of Co and Ni into the electrolyte induced the enrichment of Cr in the passive films. Moreover, the severer depletion of Ni and Co in the passive film on CrCoNiN alloy means that N promoted their dissolution, and further improved the enrichment of Cr, which is similar with the promoted selective dissolution of Fe by N in stainless steels [16,20]. The enrichment of Cr enhanced the stability of passive film on CrCoNiN alloy, and was responsible for its higher corrosion resistance. On the other hand, based on the deconvolution of XPS spectra (Fig. 9(a)), the contents of Cr_2O_3 in

Table 4
Contents of Ni, Co and Cr elements in the passive films on medium-entropy alloys (at%).

Elements	Alloys	Etching time (s)			
		0	10	20	30
Ni	CrCoNi	5.75	25.06	31.66	31.14
	CrCoNiN	7.74	17.28	26.49	32.53
Co	CrCoNi	4.51	21.85	29.26	33.92
	CrCoNiN	3.24	13.20	18.36	24.28
Cr	CrCoNi	8.24	21.02	18.03	16.36
	CrCoNiN	8.44	23.92	23.10	19.36

passive film were also enhanced by adding nitrogen, which could improve the stability and protective ability of the passive film on CrCoNiN alloy [53].

Furthermore, nitrogen itself also made great contributions to the enhancement of corrosion resistance. The spectra (Fig. 8) together with the peak areas (Fig. 9(b)) of N 1s reveal the enrichment of ammonia (NH_3 and NH_4^+) on the outmost surface of passive film and CrN at the metal/film interface on CrCoNiN alloy. The surface enrichment of NH_3 and NH_4^+ is also reported in nitrogen-alloyed stainless steels [15,21,47]. It is widely accepted that the formation of NH_3 and NH_4^+ could consume protons and enhance the pH value in incipient pits, thus promoting the repassivation of pits [21,25,27,47,54], which agrees well with the higher repassivation potential of CrCoNiN alloy (Fig. 3(c) and (d)). On the other hand, based on the adsorption mechanism [19,55], the passive film was corroded by the absorbed Cl^- ions. The N‴ (CrN) in the metal/film interface would induce desorption of Cl^- ions with the further thinning of passive film, thereby inhibiting the chlorination enhanced corrosion [19]. Moreover, the enriched CrN could improve the passive film by Eq. (2) [24,25,47,56]:

$$2CrN + 3H_2O_{ads} = Cr_2O_3 + 2NH_3(ligand) \quad (2)$$

which induced the formation of Cr_2O_3, NH_3 and even NH_4^+ with further protonation [47]. Willenbruch et al. considered the enriched CrN beneath the passive film as a precursor to the formation of passive film [56]. Therefore, the addition of nitrogen contributed to the formation of thicker and more compact passive film of CrCoNiN alloy, and thus decreased the corrosion current density, enhanced the pitting potential, repassivation potential and CPT value.

4.2. *Effect of nitrogen on the breakdown of passive film*

The Mott-Schottky analyses show that the passive films on both alloys behaved as a *p*-type semiconductor, which was closely connected with the composition of the passive films [57]. Previous studies have shown that the passive film rich in Cr_2O_3, $Cr(OH)_3$, NiO, FeO, etc. behaves as a *p*-type semiconductor, and the passive film rich in Fe_2O_3, CrO_3, etc. behaves as an *n*-type semi-

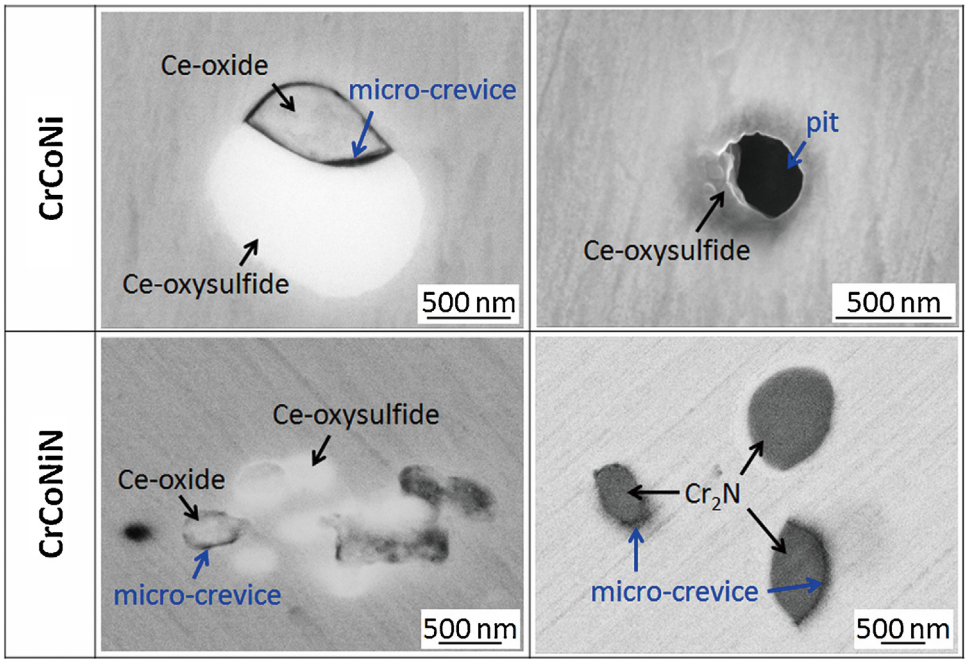

Fig. 11. Morphologies of pitting initiation sites of CrCoNi and CrCoNiN medium-entropy alloys.

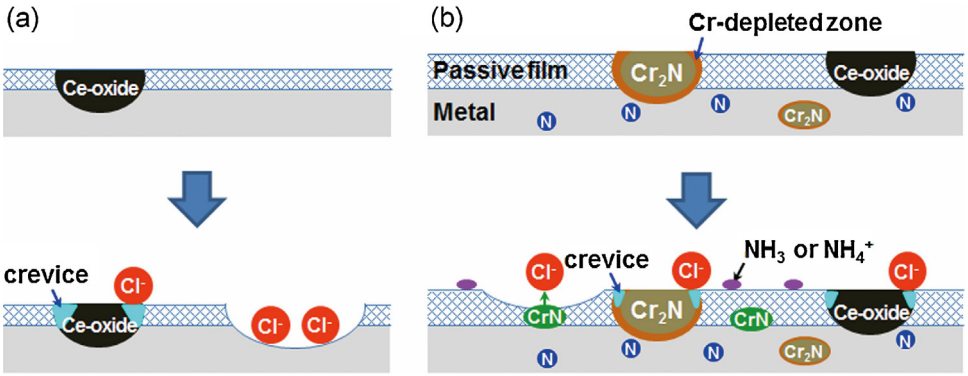

Fig. 12. Schematic diagrams of corrosion mechanism of (a) CrCoNi and (b) CrCoNiN medium-entropy alloys.

conductor [53,58]. In the present study, XPS results imply that the passive films were enriched in oxides and hydroxides of Cr, Co and Ni, and their *p*-type semiconductivity is consistent with the Mott-Schottky results. According to the point defect model (PDM) proposed by Macdonald [43,59,60], the oxygen vacancies ($V_{\ddot{O}}$) and cation interstitials (M_i^{x+}) were created at the metal/film interface, and cation vacancies ($V_M^{x'}$) were created at the film/electrolyte interface. Afterwards, they migrated and diffused across the passive film, and finally annihilated at the opposite interfaces (Fig. 10). The increasing of temperature significantly increased the generation rate (Reaction 4) and diffusivity of cation vacancies but decreased their annihilation rate (Reaction 1) [61], which induced the condensation of cation vacancies at the metal/film interface. Thereafter, the passive film detached locally from the metal and ceased to grow, whereas it continued to dissolve at the film/electrolyte interface, which would result in the breakdown of passive film and the initiation of pitting corrosion [59,61]. The above processes agree well with the higher acceptor density and lower passive film stability of CrCoNi alloy in the present work.

However, in CrCoNiN alloy, the acceptor density was remarkably reduced, in accordance with its higher Cr''' (Cr_2O_3+$Cr(OH)_3$) concentration (Fig. 9(a)). Moreover, the generation of nitrogen ions (N'''), confirmed by the enrichment of CrN at the metal/film interface (Fig. 9(b)), could consume cation vacancies by Reaction 9. At the film/electrolyte interface, N''' could react with the H^+ formed by Reaction 6, thus consuming the oxygen vacancies and enhancing the content of O_O (Reaction 10). This coincides with the higher oxygen content in CrCoNiN than CrCoNi alloy in the present study and the result by Wang et al. [62]. The formation of NH_3 could consume H^+ (Reaction 11), and reduce the corroding of the passive film. Moreover, the lower oxygen vacancy density could also restrain the adsorption of Cl^- (Reaction 8). The addition of nitrogen in CrCoNi alloy significantly decreased the density of point defects, and then decreased the breakdown susceptibility of passive film. As a consequence, the stability of passive film was enhanced, in turn, resulting in the improvement of the corrosion resistance.

4.3. *Effect of nitrogen on the metastable pitting*

To investigate the effect of nitrogen alloying on metastable pitting behaviour of CrCoNi medium-entropy alloys, the morphologies of two alloys after cyclic polarization tests in 3.5 wt% NaCl solution at 30 °C were observed using FE-SEM, as shown in Fig. 11. The micro-crevice was observed around Ce-oxide inclusion in CrCoNi

alloy, but no crevice existed around Ce-oxysulfide inclusion. This reveals that metastable pitting preferentially initiated around the Ce-oxide inclusions, and the micro-crevice might propagate to become stable pits [32]. Recently, Liu et al. [63] reported that pitting corrosion in Q460NH weathering steel initiated by the dissolution of $(RE)_2O_2S$-$(RE)_xS_y$ inclusions due to their lower Volta potential. In the present study, the preferential initiation of pitting corrosion around Ce-oxide might also associate with its lower Volta potential, and the work will be conducted in our further study.

In CrCoNiN alloy, the metastable pitting corrosion around Ce-oxide was also observed (Fig. 11). With the same deoxidization and desulfurization process, the inclusions in both alloys were almost identical, which would induce similar metastable pitting susceptibility. Meanwhile, the micro-crevices were found around Cr_2N precipitates as well. In general, the Cr-rich precipitates are detrimental to corrosion resistance due to the formation of Cr-depleted zones [21,28]. Besides, the high-density dislocation piled up around Cr_2N (Fig. 1(f)) could reduce the energy barrier for electrochemical reactions, provide more active sites, and hence increase the corrosion rate [64]. However, in this study, CrCoNiN alloy exhibited the lower metastable pitting susceptibility. The reasons can be summarized as two groups: firstly, nitrogen in the solid solution could react as NH_3 and increase the pH value on the film/electrolyte interface, which inhibited the generation of metastable pitting. Secondly, a passive film with fewer defects can cover CrCoNiN alloy surface, subsequently, resulting in the lower metastable pitting susceptibility, which can be attributed to the higher Cr content of CrCoNiN alloy.

The corrosion mechanisms of CrCoNi and CrCoNiN medium-entropy alloys are schematically presented in Fig. 12. In CrCoNi alloy, metastable pitting initiated around Ce-oxides in chloride solution, especially at high temperatures, and the passive film dissolved due to the adsorption of chloride ions. For CrCoNiN alloy, firstly, nitrogen atoms improved the corrosion resistance of both Cr-depleted zones and the matrix around the inclusions. Moreover, the thicker, less defective and more compact passive film enhanced its stability and protective ability. In addition, the generation of ammonia on the outmost surface of passive film and CrN at the metal/film interface could buffer local pH and repel chloride ions, respectively. The above effects by nitrogen alloying through pressurized metallurgy decreased the metastable pitting susceptibility and increased the corrosion resistance of CrCoNi alloy.

5. Conclusions

In this study, the effects of nitrogen alloying on microstructure and pitting corrosion resistance of CrCoNiN medium-entropy alloy were investigated. The main conclusions could be obtained as follows:

1. Nitrogen existed in the form of Cr_2N precipitates and uniformly distributed N atoms, and the addition of nitrogen significantly refined the grain size of CrCoNiN alloy.
2. Nitrogen alloying inhibited the initiation of metastable pitting, remarkably decreased corrosion current densities, increased the pitting and repassivation potentials and CPT values of CrCoNiN alloy. Metastable pitting initiated around Ce-oxide inclusions and Cr_2N precipitates.
3. The passive films on both alloys exhibited *p*-type semiconductor behaviour. The addition of nitrogen decreased the acceptor density, increased the thickness of passive film and promoted the enrichment of Cr and Cr_2O_3 in the passive film. Meanwhile, the enrichment of ammonia (NH_3 and NH_4^+) on the outmost surface of passive film and CrN at the metal/film interface on CrCoNiN alloy enhanced the protective ability of passive film.

Acknowledgements

This work was supported by the National Natural Science Foundation of China (Grant Nos. 51434004, U1435205, 51774074) and the Transformation Project of Major Scientific and Technological Achievements in Shenyang (Grant No. Z17-5-003). We acknowledge Prof. Wenqing Liu for APT experiment support and relevant discussion.

References

[1] J.W. Yeh, S.K. Chen, S.J. Lin, J.Y. Gan, T.S. Chin, T.T. Shun, C.H. Tsau, S.Y. Chang, Adv. Eng. Mater. 6 (2004) 299–303.
[2] Y. Zhang, T.T. Zuo, Z. Tang, M.C. Gao, K.A. Dahmen, P.K. Liaw, Z.P. Lu, Prog. Mater. Sci. 61 (2014) 1–93.
[3] J.W. Yeh, Ann. Chim. Sci. Mater. 31 (2006) 633–648.
[4] F. Otto, A. Dlouhy, C. Somsen, H. Bei, G. Eggeler, E.P. George, Acta Mater. 61 (2013) 5743–5755.
[5] B. Gludovatz, A. Hohenwarter, K.V.S. Thurston, H. Bei, Z. Wu, E.P. George, R.O. Ritchie, Nat. Commun. 7 (2016) 10602.
[6] H. Jiang, L. Jiang, D. Qiao, Y. Lu, T. Wang, Z. Cao, T. Li, J. Mater. Sci. Technol. 33 (2017) 712–717.
[7] C. Zhang, F. Zhang, H. Diao, M.C. Gao, Z. Tang, J.D. Poplawsky, P.K. Liaw, Mater. Des. 109 (2016) 425–433.
[8] G. Laplanche, A. Kostka, C. Reinhart, J. Hunfeld, G. Eggeler, E.P. George, Acta Mater. 128 (2017) 292–303.
[9] I. Moravcik, J. Cizek, Z. Kovacova, J. Nejezchlebova, M. Kitzmantel, E. Neubauer, I. Kubena, V. Hornik, I. Dlouhy, Mater. Sci. Eng. A 701 (2017) 370–380.
[10] Y.L. Zhao, T. Yang, Y. Tong, J. Wang, J.H. Luan, Z.B. Jiao, D. Chen, Y. Yang, A. Hu, C.T. Liu, J.J. Kai, Acta Mater. 138 (2017) 72–82.
[11] Z. Wang, I. Baker, Mater. Lett. 180 (2016) 153–156.
[12] Z. Wang, I. Baker, Z. Cai, S. Chen, J.D. Poplawsky, W. Guo, Acta Mater. 120 (2016) 228–239.
[13] C.P. Lee, Y.Y. Chen, C.Y. Hsu, J.W. Yeh, H.C. Shih, J. Electrochem. Soc. 154 (2007) C424–C430.
[14] C.L. Briant, R.A. Mulford, E.L. Hall, Corrosion 38 (1982) 468–477.
[15] Y. Fu, X.Q. Wu, E.H. Han, W. Ke, K. Yang, Z.H. Jiang, Electrochim. Acta 54 (2009) 4005–4014.
[16] J.B. Lee, S.I. Yoon, Mater. Chem. Phys. 122 (2010) 194–199.
[17] H.B. Li, E.Z. Zhou, Y.B. Ren, D.W. Zhang, D.K. Xu, C.G. Yang, H. Feng, Z.H. Jiang, X.G. Li, T.Y. Gu, K. Yang, Corros. Sci. 111 (2016) 811–821.
[18] H.B. Li, Z.H. Jiang, H. Feng, S.C. Zhang, L. Li, P.D. Han, R.D.K. Misra, J.Z. Li, Mater. Des. 84 (2015) 291–299.
[19] G. Lothongkum, P. Wongpanya, S. Morito, T. Furuhara, T. Maki, Corros. Sci. 48 (2006) 137–153.
[20] S.J. Pawel, E.E. Stansbury, C.D. Lundin, Corrosion 45 (1989) 125–133.
[21] Z.H. Jiang, H. Feng, H.B. Li, H.C. Zhu, S.C. Zhang, B.B. Zhang, Y. Han, T. Zhang, D.K. Xu, Materials 10 (2017) 861.
[22] X. Qi, H. Mao, Y. Yang, Corros. Sci. 120 (2017) 90–98.
[23] R.F.A. Jargelius-Pettersson, Corros. Sci. 41 (1999) 1639–1664.
[24] H.Y. Ha, T.H. Lee, S.J. Kim, Electrochim. Acta 80 (2012) 432–439.
[25] P.R. Levey, A. Vanbennekom, Corrosion 51 (1995) 911–921.
[26] C. Kowanda, M.O. Speidel, Scripta Mater. 48 (2003) 1073–1078.
[27] H.B. Li, Z.H. Jiang, Y. Cao, Z.R. Zhang, Int. J. Min. Met. Mater. 16 (2009) 387–392.
[28] H.B. Li, W.C. Jiao, H. Feng, Z.H. Jiang, C.D. Ren, Acta Metall. Sin. (Engl. Lett.) 29 (2016) 1148–1160.
[29] X.L. Wu, xlwu@imech.ac.cn, private communication, Beijing, October 2017.
[30] J. Liu, T. Zhang, G. Meng, Y. Shao, F. Wang, Corros. Sci. 91 (2015) 232–244.
[31] Database for surface spectroscopies as XPS, AES and UPS, http://www.lasurface.com, October 10, 2017.
[32] G. Frankel, J. Electrochem. Soc. 145 (1998) 2186–2198.
[33] H.B. Li, Z.H. Jiang, H. Feng, Q. Wang, W. Zhang, G.W. Fan, G.P. Li, L.Y. Wang, Int. J. Electrochem. Sci. 10 (2015) 1616–1631.
[34] W. Zhang, L.Z. Jiang, J.C. Hu, S.H. Mei, Mater. Sci. Eng. A 497 (2008) 501–504.
[35] M.H. Moayed, N.J. Laycock, R.C. Newman, Corros. Sci. 45 (2003) 1203–1216.
[36] L. Zhang, Y. Jiang, B. Deng, W. Zhang, J. Xu, J. Li, Mater. Charact. 60 (2009) 1522–1528.
[37] H. Tan, Z. Wang, Y. Jiang, D. Han, J. Hong, L. Chen, L. Jiang, J. Li, Corros. Sci. 53 (2011) 2191–2200.
[38] Z.J. Liu, X.Q. Cheng, S.J. Lu, X.G. Li, Acta Metall. Sin. (Engl. Lett.) 23 (2010) 431–438.
[39] G. Meng, Y. Li, Y. Shao, T. Zhang, Y. Wang, F. Wang, J. Mater. Sci. Technol. 30 (2014) 253–258.
[40] T. Zhang, Y. Shao, G. Meng, Y. Li, F. Wang, Electrochim. Acta 52 (2006) 1323–1328.
[41] Y. Qiao, X. Cai, J. Cui, H. Li, Adv. Mater. Sci. Eng. 2016 (2016) 6065481.
[42] Z. Cui, L. Wang, H. Ni, W. Hao, C. Man, S. Chen, X. Wang, Z. Liu, X. Li, Corros. Sci. 118 (2017) 31–48.
[43] H.Y. Ha, H.J. Jang, H.S. Kwon, S.J. Kim, Corros. Sci. 51 (2009) 48–53.
[44] R. Jiang, Y. Wang, X. Wen, C. Chen, J. Zhao, Appl. Surf. Sci. 412 (2017) 214–222.
[45] S. Mischler, A. Vogel, H.J. Mathieu, D. Landolt, Corros. Sci. 32 (1991) 925–944.
[46] J.B. Huang, X.Q. Wu, E.H. Han, Corros. Sci. 52 (2010) 3444–3452.
[47] C.O.A. Olsson, Corros. Sci. 37 (1995) 467–479.

[48] I. Olefjord, L. Wegrelius, Corros. Sci. 38 (1996) 1203–1220.
[49] C.G. Lee, H.Y. Ha, T.H. Lee, K.M. Cho, J. Electrochem. Soc. 164 (2017) C591–C597.
[50] L. Liu, Y. Li, F. Wang, J. Mater. Sci. Technol. 26 (2010) 1–14.
[51] C.R. Clayton, K.G. Martin, High Nitrogen Steels - HNS 88, Institute of Metals, Lille, 1988, pp. 256–260.
[52] J. Robertson, Corros. Sci. 29 (1989) 1275–1291.
[53] Y. Yang, X. Ning, H. Tang, L. Guo, H. Liu, Appl. Surf. Sci. 320 (2014) 274–280.
[54] K. Osozawa, N. Okato, Passivity and Breakdown on Iron and Iron Based Alloys, NACE, Honolulu, 1976, pp. 135–139.
[55] H.J. Grabke, ISIJ Int. 36 (1996) 777–786.
[56] R.D. Willenbruch, C.R. Clayton, M. Oversluizen, D. Kim, Y. Lu, Corros. Sci. 31 (1990) 179–190.
[57] N.E. Hakiki, Corros. Sci. 53 (2011) 2688–2699.
[58] L.Q. Guo, M.C. Lin, L.J. Qiao, A.A. Volinsky, Corros. Sci. 78 (2014) 55–62.
[59] D.D. Macdonald, J. Electrochem. Soc. 139 (1992) 3434–3449.
[60] D.D. Macdonald, Electrochim. Acta 56 (2011) 1761–1772.
[61] K. Park, S. Ahn, H. Kwon, Electrochim. Acta 56 (2011) 1662–1669.
[62] K.S. Wang, S. Tong, M.K. Lei, J. Electrochem. Soc. 162 (2015) C601–C609.
[63] C. Liu, R.I. Revilla, Z. Liu, D. Zhang, X. Li, H. Terryn, Corros. Sci. 129 (2017) 82–90.
[64] T. Balusamy, T.S.N. Sankara Narayanan, K. Ravichandran, I.S. Park, M.H. Lee, Corros. Sci. 74 (2013) 332–344.